Supporting Information

von Castelmur et al. 10.1073/pnas.1200697109

SI Text

SI Methods. ***Cloning.*** TwcKR (residues 6108–6685; UniProtKB Q23551) and its sub-fragments (except kin-CRD, see below) were cloned into the expression vector pETM-11 (EMBL collection) using KpnI and NcoI restriction sites. This vector incorporates a His_6-tag and a TEV protease cleavage site N-terminal to the target construct. Because the DNA of TwcKR contains an internal recognition sequence for NcoI, the primers were designed to use BsmBI and KpnI for restriction digestion. These sites yielded overhangs compatible with the pETM-11 vector that had been digested with NcoI and KpnI. (To ease structural annotation, residue 6,108 is considered here as residue 1).

The construct Kin-CRD was amplified from the TwcKR plasmid and cloned through NcoI/Acc65I sites into the pETM-13 vector that incorporates a C-terminal His_6-tag into the protein. To overcome problems derived from the internal NcoI site, a PciI restriction site was introduced in position 5′ of the construct and the digested fragment ligated into the NcoI site of the plasmid.

Protein production. TwcKR was expressed in *Escherichia coli* BL21 (*DE3*) Rosetta2 (Novagen). Cultures were grown at 30 °C up to an OD_{600} of 0.6 in Luria Bertani medium supplemented with 25 μg/mL kanamycin and 34 μg/mL chloramphenicol. Expression was induced with 0.5 mM IPTG and cultures grown for further 18 h at 20 °C. Cells were harvested by centrifugation. Bacterial pellet was resuspended in lysis buffer (50 mM Tris pH 7.9, 500 mM NaCl, 2 mM β-ME) containing protease inhibitors (Roche). Lysis used French pressing in the presence of DNAse I. The homogenate was clarified by centrifugation and affinity purified using a Ni^{2+}-chelating HistrapHP column (GE Healthcare) equilibrated in lysis buffer. Elution used 200 mM imidazole. Tag removal was by incubation with TEV protease overnight at 4 °C during dialysis against 50 mM Tris pH 7.9, 200 mM NaCl, 2 mM β-ME. A final purification step used subtractive metal affinity. The protein, approximately 98% pure as judged by SDS-PAGE, was concentrated by ultrafiltration while the buffer exchanged to 50 mM Tris pH 7.9, 50 mM NaCl, 2 mM DTT. The protein was stored at 4 °C until further use. The yield of pure protein was approx. 60 mg/L culture.

Crystal structure determination. Crystals of TwcKR were grown at 20 °C in sitting-drops using 96-well plates. Drops consisted of 1 μL protein solution at 24 mg/mL and 1 μL mother liquor containing 20% PEG 600, 100 mM sodium citrate pH 5.5, 50 mM $MgCl_2$. Crystals exhibited a thin-plate morphology with approximately dimensions of $0.3 \times 0.15 \times 0.05$ mm^3 and formed clusters from which single crystals were excised. For X-ray data collection, crystals were cryoprotected in mother liquor supplemented with 20% PEG 400 and shock frozen in liquid nitrogen.

X-ray diffraction data were collected at 100 K on beamline I02 at Diamond (Didcot, United Kingdom). Data were processed in XDS/XSCALE (1). Processing statistics and crystal parameters are given in Table 1 in the main text. Phasing was by molecular replacement (MR) in Phaser (2) using PDB entry 1KOA (3) as search model for the kinase and Ig^{26} domains that were treated independently. Domain Fn^{A170} from titin [2NZI; (4)] was used as search model for Fn^{31} (43% sequence identity). The MR composite model was initially improved in ARP/wARP (5) using free dummy atoms. Subsequent rebuilding used cycles of manual building in COOT (6) and TLS refinement in Phenix (7). Solvent building was in Phenix and ordered components of the crystallization buffer were modeled in COOT. The completed model was optimized with PDB_REDO (8), using Refmac with local NCS restraints (9). The final models of the two molecular copies in the asymmetric unit were virtually identical [0.56 Å rmsd for 556 Cα-atoms calculated with SPDBV; (10)]. Refinement and model statistics are given in Table 1 in the main text. The final model contains all protein residues at exception of the 104-RKRRR-108 motif in copy A and 4 and 10 residues at the N and C terminus, respectively, that were disordered. Model coordinates and diffraction data have been deposited with the Protein Data Bank (accession code 3UTO).

Phosphorylation assays. In vitro phosphorylation was assayed in 20 μL of assay buffer (20 mM Tris pH 7.4, 10 mM Mg^{2+}-acetate, 0.05% Tergitol-type NP40, 0.1 mM DTT, 0.2 mg/mL BSA) containing 0.4 mM ATP (0.2 μCi/reaction of [γ-^{33}P]ATP), 30 ng/mL recombinant kinase and 0.2 mg/mL peptide substrate at room temperature. The peptide substrate had sequence KKRARAATSNVFS and derived from chicken smooth muscle regulatory myosin light chain (kMLC 11–23) (11). At indicated time points, 5 μL of reaction mixture was withdrawn and spotted on P81 phosphocellulose paper (Whatman). The paper was washed (5×10 min) with 75 mM orthophosphoric acid and finally once with ethanol, air dried and exposed to phosphoscreen. The screen was imaged with Fujifilm BAS 2500 phosphoimager. Background subtraction and spot intensity quantification used AIDA software. Control measurements in the absence of peptide substrate showed no counts and, thus, that measurements where not the result of autophosphorylation.

X-Ray solution scattering. SAXS data were collected on the EMBL beamline X33 (DESY, Hamburg) using a photon counting Pilatus 1 M detector (DECTRIS, Switzerland). Samples were measured at solute concentrations of 1.4, 2.5, 4.1, and 6.1 mg/mL. The scattering intensity I in the range of momentum transfer $0.01 < s < 0.45$ $Å^{-1}$ was recorded ($s = 4\pi \sin\theta/\lambda$, where $\lambda = 1.5$ Å is the X-ray wavelength and 2θ is the scattering angle) at a sample-detector distance of 2.7 m. Radiation damage, monitored by repetitive 15 s exposures, was negligible. Background scattering was subtracted and data reduced, normalized, and extrapolated to infinite dilution using PRIMUS (12). Also in PRIMUS, the forward scattering I(0) and the radius of gyration R_g were evaluated using the Guinier approximation. These parameters were also computed from the entire scattering patterns using the indirect transform package GNOM (13), providing also the pair distribution function of the particle p(r) and the maximum size D_{max}. The molecular mass (MM) was estimated from I(0) by normalization against reference solutions of bovine serum albumin and it indicated that TwcKR is mostly monomeric in solution in this concentration range.

Ab initio models were created in GASBOR (14), where a simulated annealing algorithm is employed to construct a model with a "chain"-like distribution of beads that provides the best fit to the experimental data. The results of multiple GASBOR runs (20 runs) were averaged to determine common structural features using the programs DAMAVER (15) and SUPCOMB (16). The scattering pattern of the crystallographic model of TwcKR was calculated using CRYSOL (17). SASREF (18) was employed to calculate a model of TwcKR by rigid body refinement of individual domain components against SAXS data. For this calculation, the crystal structure was fragmented into Fn^{31}, β-hairpin, Nlinker crown, kinase, and Ig^{26} as well as groups of these. The flexibility of the N-terminal region was assessed by an ensemble

optimization method (EOM) (19). Coexisting conformers were selected using a genetic algorithm from a pool containing a large number of randomly generated models. An ensemble pool of 10^5 structures (where Fn^{31} was connected by a flexible loop of eight residues to the NL-kinase-CRD-Ig^{26} fraction of TwcKR) was generated to find the mixture of conformer models that fitted the experimental data. Multiple runs of EOM and the obtained subsets were analyzed to yield the R_g distributions in the optimum ensembles.

Molecular dynamic simulations. The atomic coordinates of TwcKR (or its kinase core fraction) were placed in ionized water boxes containing Na^+ and Cl^- ions at a concentration of 0.3 mol/l. The water boxes had sizes that accommodated the stretched molecular conformations. Each system was initially equilibrated for 10 ns, holding the Cα-atoms of the N- and C-terminal residues fixed to preserve protein orientation. Altogether, the TwcKR system included 510′000 atoms (box size $605 \times 96 \times 88$ Å^3) and was simulated for a total time of 100 ns (including equilibration time). The kinase-CRD system contained 553′000 atoms in a solvation box of $865 \times 87 \times 74$ Å^3 and was simulated for a total of 74 ns.

All MDS were performed using NAMD 2.7 (20) and analyzed with VMD 1.9 (21). The CHARMM22 (22) force field with CMAP corrections (23) was employed and the TIP3P (24) model used for water molecules. Van der Waals interaction cutoff distances were set at 12 Å (smooth switching function beginning at 10 Å) and long-range electrostatic forces were computed using the particle-mesh Ewald (PME) summation method (25) with a grid size of 1 Å. For equilibrium simulations, constant temperature ($T = 300$ K) was enforced using Langevin dynamics with a damping coefficient of 1 ps^{-1}, and constant pressure ($p = 1$ atm) enforced through the Nosé-Hoover Langevin piston method with a decay period of 100 fs and a damping time constant of 50 fs. Force-responses were probed by SMD simulations (26), which fixed the Cα-atom at the molecular N terminus and applied a spring force to that at the C terminus. The constant velocity stretching protocol (as described in refs. 27, 28) was used with a constant velocity of 5 Å/ns and a spring constant of $3k_BT/$Å^2. Iterative truncation procedures were not applied.

1. Kabsch W (1993) Automatic processing of rotation diffraction data from crystals of initially unknown symmetry and cell constants. *J Appl Cryst* 26:795–800.
2. McCoy AJ, et al. (2007) Phaser crystallographic software. *J Appl Crystallogr* 40:658–674.
3. Kobe B, et al. (1996) Giant protein kinases: Domain interactions and structural basis of autoregulation. *EMBO J* 15:6810–6821.
4. Mrosek M, et al. (2007) Molecular determinants for the recruitment of the ubiquitin-ligase MuRF-1 onto M-line titin. *FASEB J* 21:1383–1392.
5. Perrakis A, Harkiolaki M, Wilson KS, Lamzin VS (2001) ARP/wARP and molecular replacement. *Acta Crystallogr D* 57:1445–1450.
6. Emsley P, Cowtan K (2004). COOT: Model-building tools for molecular graphics. *Acta Crystallogr D* 60:2126–2132.
7. Adams PD, et al. (2002) PHENIX: Building new software for automated crystallographic structure determination. *Acta Crystallogr D* 58:1948–1954.
8. Joosten RP, Womack T, Vriend G, Bricogne G (2009) Re-refinement from deposited X-ray data can deliver improved models for most PDB entries. *Acta Crystallogr D* 65:176–185.
9. Murshudov GN, et al. (2011) REFMAC5 for the refinement of macromolecular crystal structures. *Acta Crystallogr D* 67:355–367.
10. Guex N, Peitsch MC (1997) SWISS-MODEL and the Swiss-PdbViewer: An environment for comparative protein modeling. *Electrophoresis* 18:2714–2723.
11. Heierhorst J, et al. (1996) Substrate specificity and inhibitor sensitivity of Ca2+/S100-dependent twitchin kinases. *Eur J Biochem* 242:454–459.
12. Konarev PV, Volkov VV, Sokolova AV, Koch MHJ, Svergun DI (2003) PRIMUS—a Windows-PC based system for small-angle scattering data analysis. *J Appl Crystallogr* 36:1277–1282.
13. Svergun DI (1992). Determination of the regularization parameter in indirect transform methods using perceptual criteria. *J Appl Crystallogr* 25:495–503.
14. Svergun DI, Petoukhov MV, Koch MHJ (2001) Determination of domain structure of proteins from X-ray solution scattering. *Biophys J* 80:2946–2953.
15. Volkov VV, Svergun DI (2003) Uniqueness of ab initio shape determination in small angle scattering. *J Appl Cryst* 36:860–864.
16. Kozin MB, Svergun DI (2001) Automated matching of high- and low- resolution structural models. *J Appl Cryst* 34:33–41.
17. Svergun DI, Barberato C, Koch MHJ (1995). CRYSOL- a program to evaluate X-ray solution scattering of biological macromolecules from atomic coordinates. *J Appl Crystallogr* 28:768–773.
18. Petoukhov MV, Svergun DI (2005) Global rigid body modelling of macromolecular complexes against small-angle scattering data. *Biophys J* 89:1237–1250.
19. Bernadó P, Mylonas E, Petoukhov MV, Blackledge M, Svergun DI (2007) Structural characterization of flexible proteins using small-angle X-ray scattering. *J Am Chem Soc* 129:5656–5664.
20. Phillips JC, et al. (2005) Scalable molecular dynamics with NAMD. *J Comput Chem* 26:1781–802.
21. Humphrey W, Dalke A, Schulten K (1996) VMD—Visual Molecular Dynamics. *J Mol Graphics* 14:33–38.
22. MacKerell AD, Jr., (1998) All-atom empirical potential for molecular modeling and dynamics studies of proteins. *J Phys Chem B* 102:3586–3616.
23. Mackerell AD, Jr., Feig M, Brooks CL, 3rd. (2004) Extending the treatment of backbone energetics in protein force fields: Limitations of gas-phase quantum mechanics in reproducing protein conformational distributions in molecular dynamics simulations. *J Comput Chem* 25:1400–1415.
24. Jorgensen WL, Chandrasekhar J, Madura JD, Impey RW, Klein ML (1983) Comparison of simple potential functions for simulating liquid water. *J Chem Phys* 79:926–935.
25. Darden T, York D, Pedersen L (1993) Particle mesh Ewal: An N log(N) method for Ewald sums in large systems. *J Chem Phys* 98:10089–10092.
26. Lu H, Isralewitz B, Krammer A, Vogel V, Schulten K (1998). Unfolding of titin immunoglobulin domains by steered molecular dynamics simulation. *Biophys J* 75:662–671.
27. Lee EH, Hsin J, von Castelmur E, Mayans O, Schulten K (2010) Tertiary and secondary structure elasticity of a six-Ig titin chain. *Biophys J* 98:1085–1095.
28. Hsin J, Schulten K (2011) Improved resolution of tertiary structure elasticity in muscle protein. *Biophys J* 100:L22–L24.

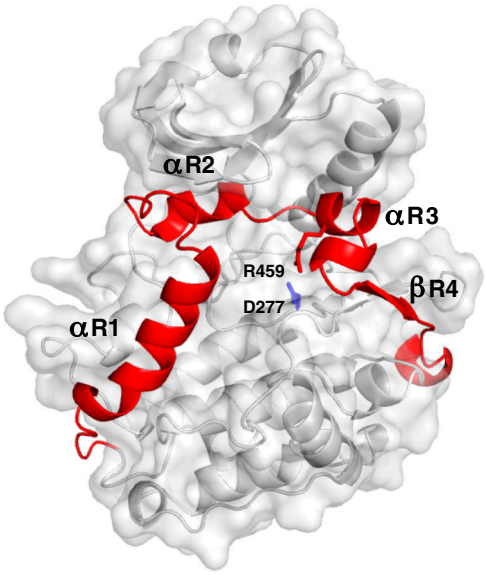

Fig. S1. Structure of the C-terminal regulatory tail domain of twitchin kinase. Secondary structure elements are labeled. The inhibitory salt bridge between the tail residue R459 and the catalytic aspartate D277 is shown. The C-terminal regulatory segment (CRD) folds into three helical segments (αR1, αR2, αR3) and a short terminal β-strand (βR4) (nomenclature as in ref. 1). Helix αR2 is of the 3_{10} type and is wedged between both kinase lobes, blocking the ATP binding site. Helix αR3, that is interrupted by a proline residue in its mid point (splitting in αR3 and αR3′), blocks the binding site of the phosphorylatable substrate and inactivates the catalytic base D277 by forming a salt bridge to its residue R459 (residue numbering defined in *Methods*). The C-terminal β-strand βR4 packs against strand βC10 from the activation loop of the kinase, forming a two-stranded antiparallel β-sheet. The CRD is followed by domain Ig^{26} that makes contact with the kinase domain. The relative position of Ig^{26} coincides with that observed previously (2) [0.74 Å rmsd for 441 shared Cα atoms in the kin-CRD-Ig^{26} fraction calculated with SPDBV; (3)], indicating that the arrangement is not merely caused by crystal packing.

1 Hu SH, et al. (1994) Insights into autoregulation from the crystal structure of twitchin kinase. *Nature* 369:581–584.
2 Kobe B, et al. (1996) Giant protein kinases: Domain interactions and structural basis of autoregulation. *EMBO J* 15:6810–6821.
3 Guex N, Peitsch MC (1997) SWISS-MODEL and the Swiss-PdbViewer: An environment for comparative protein modeling. *Electrophoresis* 18:2714–2723.

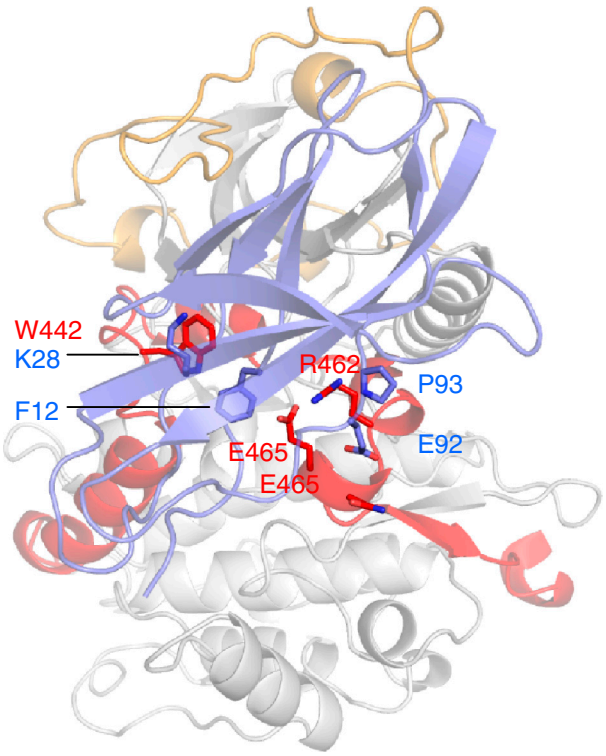

Fig. S2. Inter-modular contacts of Fn^{31} observed in the crystal structure. Crystal structure viewed from the N terminus. Structural regions are color-coded as in the main text. The residues involved in the interactions are shown amid a semi-transparent ribbon of the global fold. Direct interactions are listed below in Table S1. Two clusters of interacting residues can be identified that mediate the docking of Fn^{31} against the CRD tail: (*i*) one predominantly hydrophobic, consisting of W422, F12, and the aliphatic chain of K28; (*ii*) the other polar, where residue R462 from the CRD binds the main-chain of E92 and P83 in Fn^{31}, and the lateral carbonyl group of E92 in Fn^{31} interacts with the main chain of Q464 and E465 in the CRD.

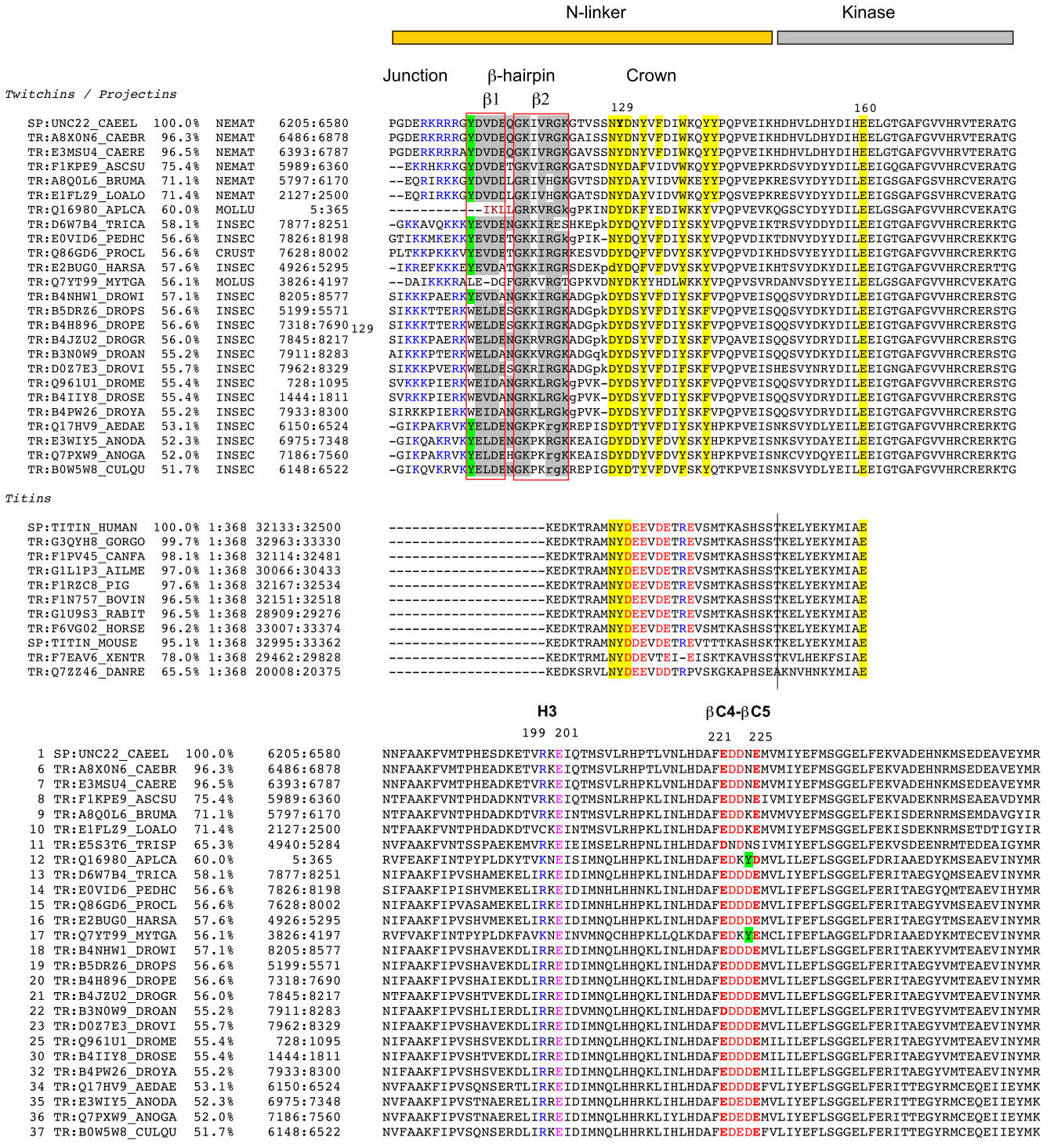
N-linker
Kinase
Junction
β-hairpin
Crown
β1
β2
129
160
Twitchins / Projectins
SP:UNC22_CAEEL 100.0% NEMAT 6205:6580 PGDERKRRRGYDVDEQGKIVRGKGTVSSNYDNYVFDIWKQYYPQPVEIKHDHVLDHYDIHEELGTGAFGVVHRVTERATG
TR:A8X0N6_CAEBR 96.3% NEMAT 6486:6878 PGDERKRRRGYDVDEQGKIVRGKGAISSNYDNYVFDIWKQYYPQPVEIKHDHVLDHYDIHEELGTGAFGVVHRVTERATG
TR:E3MSU4_CAERE 96.5% NEMAT 6393:6787 PGDERKRRRAYDVDEQGKIVRGKGAVSSNYDNYVFDIWKQYYPQPVEIKHDHVLDHYDIHEELGTGAFGVVHRVTERATG
TR:F1KPE9_ASCSU 75.4% NEMAT 5989:6360 --EKRHKRKGYDVDETGKVIRGKGATSDNYDAFVIDVWKQYYPQPVEPKRDSVYDYYDILEEIGQGAFGVVHRCVERATG
TR:A8Q0L6_BRUMA 71.1% NEMAT 5797:6170 --EQRIRKKGYDVDDLGRIVHGKGVTSDNYDAYVIDVWKEYYPQPVEPKRESVYDYDILEEIGSGAFGSVHRCVERATG
TR:E1FLZ9_LOALO 71.4% NEMAT 2127:2500 --EQRIRKKGYDVDDIGKIVHGKGATSDNYDAYVIDVWKQYYPQSVEPKRESVYDYYDILEEIGSGAFGSVHRCVERATG
TR:Q16980_APLCA 60.0% MOLLU 5:365 ----------IKILGRKVRGkgPKINDYDKFYEDIWKKYVPQPVEVKQGSCYDYYDILEELGSGAFGVVHRCVEKATG
TR:D6W7B4_TRICA 58.1% INSEC 7877:8251 -GKKAVQKKKYEVDENGKKIRESHKEpkDYDQYVFDIYSKYVPQPVEIKTRSVYDDYDILEEIGTGAFGVVHRCREKKTG
TR:E0VID6_PEDHC 56.6% INSEC 7826:8198 GTIKKMKEKKYEVDETGKKIRGkgPIK-NYDQYVFDIYSKYVPQPVDIKTDNVYDYYDILEEIGTGAFGVVHRCREKKTG
TR:Q86GD6_PROCL 56.6% CRUST 7628:8002 PLTKKPKKKVYEVDETGKKIRGRKESVDDYDQFVFDVYSKYVPQPVDIKHDSVYEYYDILEEIGTGAFGVVHRCREKRTG
TR:E2BUG0_HARSA 57.6% INSEC 4926:5295 -IKREFKKKEYEVDATGKKIRGRSDEKpdYDQFVFDVYSKYVPQPVEIKHTSVYDYDILEEIGTGAFGVVHRCRERTTG
TR:Q7YT99_MYTGA 56.1% MOLUS 3826:4197 --DAIKKKRALE-DGFGRKVRGTGPKVDNYDKYYHDLWKKYVPQPVSVRDANVSDYYEILEELGSGAFGVVHRCVEKATG
TR:B4NHW1_DROWI 57.1% INSEC 8205:8577 SIKKKPAERKYEVDANGKKIRGKADGpkDYDSYVFDIYSKFVPQPVEISQQSVYDRYDILEEIGTGAFGVVHRCRERSTG
TR:B5DRZ6_DROPS 56.6% INSEC 5199:5571 SIKKKTTERKWELDESGKKIRGKADGpkDYDSYVFDIYSKFVPQPVEISQQSVYDKYDILEEIGTGAFGVVHRCRERSTG
TR:B4H896_DROPE 56.6% INSEC 7318:7690 129 SIKKKTTERKWELDESGKKIRGKADGpkDYDSYVFDIYSKFVPQPVEISQQSVYDKYDILEEIGTGAFGVVHRCRERSTG
TR:B4JZU2_DROGR 56.0% INSEC 7845:8217 SIKKKPAERKWELDENGKRVRGKADGpkDYDSYVFDIYSKFVPQAVEISQQSVYDRYDILEEIGTGAFGVVHRCRERSTG
TR:B3N0W9_DROAN 55.2% INSEC 7911:8283 AIKKKPTERKWELDANGKKVRGKADGqkDYDSYVFDIYSKFVPQPVEISQQSVYDKYDILEEIGTGAFGVVHRCRERSTG
TR:D0Z7E3_DROVI 55.7% INSEC 7962:8329 SIKKKPVERKWELDESGKRIRGKADGpkDYDSYVFDIFSKFVPQPVEISHESVYNRYDILEEIGNGAFGVVHRCRERSTG
TR:Q961U1_DROME 55.4% INSEC 728:1095 SVKKKPIERKWEIDANGRKLRGkgPVK-DYDSYVFDIYSKFVPQPVEISQQSVYDRYDILEEIGTGAFGVVHRCRERSTG
TR:B4IIY8_DROSE 55.4% INSEC 1444:1811 SVRKKPIERKWEVDANGRKLRGkgPVK-DYDSYVFDIYSKFVPQPVEISQQSVYDRYDILEEIGTGAFGVVHRCRERSTG
TR:B4PW26_DROYA 55.2% INSEC 7933:8300 SIRKKPIERKWEIDANGRKLRGkgPVK-DYDSYVFDIYSKFVPQPVEISQQSVYDRYDILEEIGTGAFGVVHRCRERSTG
TR:Q17HV9_AEDAE 53.1% INSEC 6150:6524 -GIKPAKRVKYELDENGKPKrgKREPISDYDTYVFDIYSKYHPKPVEISNKSVYDLYEILEEIGTGAFGVVHRCRERKTG
TR:E3WIY5_ANODA 52.3% INSEC 6975:7348 -GIKQAKRVKYELDENGKPKRGKKEAIGDYDDYVFDVYSKYHPKPVEISNKSVYDAYEILEEIGTGAFGVVHRCRERKTG
TR:Q7PXW9_ANOGA 52.0% INSEC 7186:7560 -GIKPAKRVKYELDEHGKPKrgKKEAISDYDDYVFDVYSKYHPKPVEISNKCVYDQYEILEEIGTGAFGVVHRCRERKTG
TR:B0W5W8_CULQU 51.7% INSEC 6148:6522 -GIKQVKRVKYELDENGKPKrgKREPIGDYDTYVFDVFSKYQTKPVEISNKSVYDLYEILEEIGTGAFGVVHRCRERKTG
Titins
SP:TITIN_HUMAN 100.0% 1:368 32133:32500 ----------KEDKTRAMNYDEEVDETREVSMTKASHSSTKELYEKYMIAE
TR:G3QYH8_GORGO 99.7% 1:368 32963:33330 ----------KEDKTRAMNYDEEVDETREVSMTKASHSSTKELYEKYMIAE
TR:F1PV45_CANFA 98.1% 1:368 32114:32481 ----------KEDKTRAMNYDEEVDETREVSMTKASHSSTKELYEKYMIAE
TR:G1L1P3_AILME 97.0% 1:368 30066:30433 ----------KEDKTRAMNYDEEVDETREVSMTKASHSSTKELYEKYMIAE
TR:F1RZC8_PIG 97.6% 1:368 32167:32534 ----------KEDKTRAMNYDEEVDETREVSMTKASHSSTKELYEKYMIAE
TR:F1N757_BOVIN 96.5% 1:368 32151:32518 ----------KEDKTRAMNYDEEVDETREVSMTKASHSSTKELYEKYMIAE
TR:G1U9S3_RABIT 96.5% 1:368 28909:29276 ----------KEDKTRAMNYDEEVDETREVSMTKASHSKTKELYEKYMIAE
TR:F6VG02_HORSE 96.2% 1:368 33007:33374 ----------KEDKTRAMNYDEEVDETREVSMTKASHSSTKELYEKYMIAE
SP:TITIN_MOUSE 95.1% 1:368 32995:33362 ----------KEDKTRAMNYDDEVDETREVTTTKASHSKTKELYEKYMIAE
TR:F7EAV6_XENTR 78.0% 1:368 29462:29828 ----------KEDKTRMLNYDDEVTEI-EISKTKAVHSSTKVLHEKFSIAE
TR:Q7ZZ46_DANRE 65.5% 1:368 20008:20375 ----------KEDKSRVLNYDEEVDDTRPVSKGKAPHSEAKNVHNKYMIAE
H3
199 201
βC4-βC5
221 225
1 SP:UNC22_CAEEL 100.0% 6205:6580 NNFAAKFVMTPHESDKETVRKEIQTMSVLRHPTLVNLHDAFEDDNEMVMIYEFMSGGELFEKVADEHNKMSEDEAVEYMR
6 TR:A8X0N6_CAEBR 96.3% 6486:6878 NNFAAKFVMTPHEADKETVRKEIQTMSVLRHPTLVNLHDAFEDDNEMVMIYEFMSGGELFEKVADEHNRMSEDEAVEYMR
7 TR:E3MSU4_CAERE 96.5% 6393:6787 NNFAAKFVMTPHEADKETVRKEIQTMSVLRHPKLVNLHDAFEDDNEMVMIYEFMSGGELFEKVADEHNKMSEDEAVEYMR
8 TR:F1KPE9_ASCSU 75.4% 5989:6360 NTFAAKFVNTPHDADKNTVRKEIQTMSNLRHPKLINLHDAFEDDNEIVMIYEFMSGGELFEKVADEKNRMSEAEAVDYMR
9 TR:A8Q0L6_BRUMA 71.1% 5797:6170 NTFAAKFVNTPHDADKDTVRKEINTMSVLRHPKLINLHDAFEDDKEMVMVYEFMSGGELFEKISDERNRMSEMDAVGYIR
10 TR:E1FLZ9_LOALO 71.4% 2127:2500 NTFAAKFVNTPHDADKDTVCKEINTMSVLRHPKLINLHDAFEDDKEMVMIYEFMSGGELFEKISDEKNRMSETDTIGYIR
11 TR:E5S3T6_TRISP 65.3% 4940:5284 NVFAAKFVNTSSPAEKEMVRKEIEIMSELRHPNLIHLHDAFDNDNSIVMIYEFLSGGELFEKVSDEENRMTEDEAIGYMR
12 TR:Q16980_APLCA 60.0% 5:365 RVFEAKFINTPYPLDKYTVKNEISIMNQLHHPKLINLHDAFEDKYDMVLILEFLSGGELFDRIAAEDYKMSEAEVINYMR
13 TR:D6W7B4_TRICA 58.1% 7877:8251 NIFAAKFIPVSHAMEKELIRKEIDIMNQLHHPKLINLHDAFEDDDEMVLIYEFLSGGELFERITAEGYQMSEAEVINYMR
14 TR:E0VID6_PEDHC 56.6% 7826:8198 SIFAAKFIPISHVMEKELIRKEIDIMNHLHHNKLINLHDAFEDDDEMVLIFEFLSGGELFERITAEGYQMTEAEVIHYMR
15 TR:Q86GD6_PROCL 56.6% 7628:8002 NIFAAKFIPVASAMEKELIRKEIDIMNHLHHPKLINLHDAFEDDDEMVLIFEFLSGGELFERITAEGYVMSEAEVINYMR
16 TR:E2BUG0_HARSA 57.6% 4926:5295 NIFAAKFIPVSHVMEKELIRKEIDIMNQLHHPKLINLHDAFEDDDEMVLIFEFLSGGELFERITAEGYTMSEAEVINYMR
17 TR:Q7YT99_MYTGA 56.1% 3826:4197 RVFVAKFINTPYPLDKFAVKNEINVMNQCHHPKLLQLKDAFEDKYEMCLIFEFLAGGELFDRIAAEDYKMTECEVINYMR
18 TR:B4NHW1_DROWI 57.1% 8205:8577 NIFAAKFIPVSHAVEKDLIRREIDIMNQLHHQKLINLHDAFEDDDEMVLILEFLSGGELFERITAEKYVMTEAEVINYMR
19 TR:B5DRZ6_DROPS 56.6% 5199:5571 NIFAAKFIPVSHAVEKDLIRREIDIMNQLHHQKLINLHDAFEDDDEMVLILEFLSGGELFERITAEGYVMTEAEVINYMR
20 TR:B4H896_DROPE 56.6% 7318:7690 NIFAAKFIPVSHAIEKDLIRREIDIMNQLHHQKLINLHDAFEDDDEMVLILEFLSGGELFERITAEGYVMTEAEVINYMR
21 TR:B4JZU2_DROGR 56.0% 7845:8217 NTFAAKFIPVSHTVEKDLIRREIDIMNQLHHQKLINLHDAFEDDDEMVLILEFLSGGELFERITAEGYVMTEAEVINYMR
22 TR:B3N0W9_DROAN 55.2% 7911:8283 NIFAAKFIPVSHLIERDLIRREIDVMNQLHHQKLINLHDAFDDDDEMVLILEFLSGGELFERITVEGYVMTEAEVINYMR
23 TR:D0Z7E3_DROVI 55.7% 7962:8329 NIFAAKFIPVSHAVEKDLIRREIDIMNQLHHQKLINLHDAFEDDDEMVLILEFLSGGELFERITAEGYVMTEAEVINYMR
25 TR:Q961U1_DROME 55.4% 728:1095 NIFAAKFIPVSHSVEKDLIRREIDIMNQLHHQKLINLHDAFEDDDEMILILEFLSGGELFERITAEGYVMTEAEVINYMR
30 TR:B4IIY8_DROSE 55.4% 1444:1811 NIFAAKFIPVSHTVEKDLIRREIDIMNQLHHQKLINLHDAFEDDDEMILILEFLSGGELFERITAEGYVMTEAEVINYMR
32 TR:B4PW26_DROYA 55.2% 7933:8300 NIFAAKFIPVSHSVEKDLIRREIDIMNQLHHQKLINLHDAFEDDDEMILILEFLSGGELFERITAEGYVMTEAEVINYMR
34 TR:Q17HV9_AEDAE 53.1% 6150:6524 NVFAAKFIPVSQNSERTLIRKEIDIMNQLHHRKLIHLHDAFEDDDEFVLIYEFLSGGELFERITTEGYRMCEQEIIEYMK
35 TR:E3WIY5_ANODA 52.3% 6975:7348 NVFAAKFIPVSTNAERELIRREIDIMNQLHHRKLIHLHDAFEDEDEMVLIYEFLSGGELFERITTEGYRMCEQEIIEYMK
36 TR:Q7PXW9_ANOGA 52.0% 7186:7560 NVFAAKFIPVSTNAERELIRREIDIMNQLHHRKLIYLHDAFEDEDEMVLIYEFLSGGELFERITTEGYRMCEQEIIEYMK
37 TR:B0W5W8_CULQU 51.7% 6148:6522 NVFAAKFIPVSQNSERDLIRKEIDIMNQLHHRKLIHLHDAFEDEDEFVLIYEFLSGGELFERITTEGYRMCEQEIIEYMK

1	SP:UNC22_CAEEL	100.0%	6205:6580	QVCKGLCHMHENNYVHLDLKPENIMFTTKRSNELKLIDFGLTAHLDPKQSVKVTTGTAEFAAPEVAEGKPVGYYTDMWSV
6	TR:A8X0N6_CAEBR	96.3%	6486:6878	QVCKALCHMHENNYVHLDLKPENIMFTTKRSNELKLIDFGLTAHLDPKQSVKVTTGTAEFAAPEVAEGKPVGYYTDMWSV
7	TR:E3MSU4_CAERE	96.5%	6393:6787	QVCKALCHMHENNYVHLDLKPENIMFTTKRSNELKLIDFGLTAHLDPKQSVKVTTGTAEFAAPEVAEGKPVGYYTDMWSV
8	TR:F1KPE9_ASCSU	75.4%	5989:6360	QVCDALRHMHEMNYVHLDLKPENIMFTTKKSNQLKLIDFGLAAKLDPKETVKVTTGTAEFAAPEVAASKPVGFYTDMWSV
9	TR:A8Q0L6_BRUMA	71.1%	5797:6170	QICEALCHMHEMSYVHLDLKPENIMFITKKSDQLKLIDFGLAAKLDPRDTVKVTTGTAEFAAPEVVANEPVGYYTDMWSV
10	TR:E1FLZ9_LOALO	71.4%	2127:2500	QVCEALRHMHEMNYVHLDLKPENIMFMTKKSDQLKLIDFGLAAKLDPKDTVKVTTGTAEFAAPEVVANEPVGFYTDMWSI
11	TR:E5S3T6_TRISP	65.3%	4940:5284	QVCEGLAHMHERNIVHLDIKPENVMFCSKNSNVLKLIDFGLAAKLNPSDIVKVTTGTAEFAAPEIVDMEPIGFYTDMWAV
12	TR:Q16980_APLCA	60.0%	5:365	QACEGLKHMHEHSIVHLDIKPENIMCETKKASSVKIIDFGLATKLNPDEIVKVTTATAEFAAPEIVDREPVGFYTDMWAI
13	TR:D6W7B4_TRICA	58.1%	7877:8251	QICEAIKHMHERNIIHLDIKPENIMCQTRKGTNIKLIDFGLATKLDPNEVVKISTGTAEFAAPEIVEREPVGFYTDMWAV
14	TR:E0VID6_PEDHC	56.6%	7826:8198	QICEAMKHMHEKNIIHLDIKPENIMCQTRNSTNIKLIDFGLATKLEPNDVVKISTGTAEFAAPEIVEREPVGFYTDMWAV
15	TR:Q86GD6_PROCL	56.6%	7628:8002	QICEGVKHMHEKNIIHLDVKPENIMCQTKTSTNVKLIDFGLATKLDPNEVVKISTGTAEFAAPEIVEREPVGFYTDMWAV
16	TR:E2BUG0_HARSA	57.6%	4926:5295	QICEGVKHMHEKNIIHLDIKPENIMCQTRNSTNVKLIDFGLATKLDPNEVVKISTGTAEFAAPEIVEREPVGFYTDMWAC
17	TR:Q7YT99_MYTGA	56.1%	3826:4197	QICDGLKHMHENSIVHLDVKPENVMCTTKNSNEVKMIDFGLATKLNPDEIVKVTTATAEFAAPEIVDREPVGFYTDMWAV
18	TR:B4NHW1_DROWI	57.1%	8205:8577	QICEGIRHMHEKNIIHLDIKPENIMCQTRSSTSVKLIDFGLATRLDPNEVVKITTGTAEFAAPEIVNREPVGFYTDMWAT
19	TR:B5DRZ6_DROPS	56.6%	5199:5571	QICEGIRHMHEKNIIHLDIKPENIMCQTRSSTNVKLIDFGLATRLDPNEVVKITTGTAEFAAPEIVNREPVGFYTDMWAT
20	TR:B4H896_DROPE	56.6%	7318:7690	QICEGIRHMHEKNIIHLDIKPENIMCQTRSSTNVKLIDFGLATRLDPNEVVKITTGTAEFAAPEIVNREPVGFYTDMWAT
21	TR:B4JZU2_DROGR	56.0%	7845:8217	QICEGIRHMHEKNIIHLDIKPENIMCQTRTSTNVKLIDFGLATRLDPNEVVKITTGTAEFAAPEIVNREPVGFYTDMWAT
22	TR:B3N0W9_DROAN	55.2%	7911:8283	QICEGLKHMHERNIIHLDIKPENIMCQTRSSTNVKLIDFGLATRLDPNEVVKITTGTAEFAAPEIVNREPVGFYTDMWST
23	TR:D0Z7E3_DROVI	55.7%	7962:8329	QICEGIRHMHEKNIIHLDIKPENIMCQTRTSTNVKLIDFGLATRLDPNEVVKITTGTAEFAAPEIVNREPVGFYTDMWAT
25	TR:Q961U1_DROME	55.4%	728:1095	QICEGIRHMHEQNIIHLDIKPENIMCQTRSSTNVKLIDFGLATRLDPNEVVKITTGTAEFAAPEIVNREPVGFYTDMWAT
26	TR:Q7KQP6_DROME	55.4%	7655:8022	QICEGIRHMHEQNIIHLDIKPENIMCQTRSSTNVKLIDFGLATRLDPNEVVKITTGTAEFAAPEIVNREPVGFYTDMWAT
27	TR:D1YSG1_DROME	55.4%	7595:7962	QICEGIRHMHEQNIIHLDIKPENIMCQTRSSTNVKLIDFGLATRLDPNEVVKITTGTAEFAAPEIVNREPVGFYTDMWAT
28	TR:D1YSG0_DROME	55.4%	7940:8307	QICEGIRHMHEQNIIHLDIKPENIMCQTRSSTNVKLIDFGLATRLDPNEVVKITTGTAEFAAPEIVNREPVGFYTDMWAT
29	TR:O76281_DROME	55.2%	5665:6032	QICEGIRHMHEQNIIHLDIKPENIMCQTRSSTNVKLIDFGLATRLDPNEVVKITTGTAEFGAPEIVNREPVGFYTDMWAT
30	TR:B4IIY8_DROSE	55.4%	1444:1811	QICEGIRHMHEQNIIHLDIKPENIMCQTRSSTNVKLIDFGLATRLDPNEVVKITTGTAEFAAPEIVNREPVGFYTDMWAT
32	TR:B4PW26_DROYA	55.2%	7933:8300	QICEGIRHMHEQNIIHLDIKPENIMCQTRSSTNVKLIDFGLATRLDPNEVVKITTGTAEFAAPEIVNREPVGFYTDMWAT
34	TR:Q17HV9_AEDAE	53.1%	6150:6524	QICEAVKYMHEKNIIHLDIKPENVMCQTRNSNQVKLIDFGLATRLNPNEMVKISTGTAEFAAPEIVEREPVGFYTDMWAV
35	TR:E3WIY5_ANODA	52.3%	6975:7348	QICEAVKYMHEKNIIHLDIKPENVMCQTRNTNQVKLIDFGLATKLNPNEMVKISTGTAEFAAPEIVEREPVGFYTDMWAV
36	TR:Q7PXW9_ANOGA	52.0%	7186:7560	QICEAVKYMHERNIIHLDIKPENVMCQTRNTNQVKLIDFGLATKLNPNEMVKISTGTAEFAAPEIVEREPVGFYTDMWAV
37	TR:B0W5W8_CULQU	51.7%	6148:6522	QICEAVKYMHEKNIIHLDIKPENVMCQTRNSNQVKLIDFGLATRLNPNEMVKISTGTAEFAAPEIVEREPVGFYTDMWAV

1	SP:UNC22_CAEEL	100.0%	6205:6580	GVLSYILLSGLSPFGGENDDETLRNVKSCDWNMDDSAFSGISEDGKDFIRKLLLADPNTRMTIHQALEHPWLTPGNAPGR
6	TR:A8X0N6_CAEBR	96.3%	6486:6878	GVLSYILLSGLSPFGGENDDDTLRNVksCDWNMDDSAFSSISEDGKDFIRKLLLADPNSRMTIHQALEHPWLSPGSVPGR
7	TR:E3MSU4_CAERE	96.5%	6393:6787	GVLSYILLSGLSPFGGENDDDTLRNVksCDWNMDDSAFSNISDDGKDFIRKLLLADPNTRMTIHQALEHPWLSPGNVPGR
8	TR:F1KPE9_ASCSU	75.4%	5989:6360	GVLAYILLSGLSPFGGETDEETLRNVKNCDWSMDDPCFAKVSDEAKDFIKKLLVLDPTSRMTVHEALEHPWLS--NAPST
9	TR:A8Q0L6_BRUMA	71.1%	5797:6170	GVLAYILLSGLSPFGGETDDETLRNVKKCDWNMDDPSFASISQDAKDFIKKILMLDPKSRMTVHEALEHPWLNGATSNVP
10	TR:E1FLZ9_LOALO	71.4%	2127:2500	GVLAYILLSGLSPFGGETDEETLRNVKKCDWNMDDPSFANISQEGKDFIMKLLMLDPKSRMTVHEALEHPWLsaNNVPSQ
11	TR:E5S3T6_TRISP	65.3%	4940:5284	GVLAYVLLSGLSPFGGETDVETLKNVKNCDWDFDPDAFKTVSDEAKDFIKKLLVRDPNCRLTVQQCLEHPWLKkeKSDFV
12	TR:Q16980_APLCA	60.0%	5:365	GVLGYVLLSGLSPFAGEDDLETLQNVKRCDWEFDEDAFSSVSPEAKDFIKNLLQKEPRKRLTVHDALEHPWL-KGDHSNL
13	TR:D6W7B4_TRICA	58.1%	7877:8251	GVLAYVLLSGLSPFAGENDIETLKNVKACDWDFDEEAFANVSEEGKDFIRRLLLKNKEKRMTAEECLLHAWLS-GDHSDK
14	TR:E0VID6_PEDHC	56.6%	7826:8198	GVLAYVLLSGLSPFAGENDVETLKNVKACDWEFDEDAFAGVSEEGKDFIRRLLIKSQEKRMTAHECLRHPWLM-GDEKSK
15	TR:Q86GD6_PROCL	56.6%	7628:8002	GVLAYVLLSGLSPFAGENDIDTLKNVKACDWDFDEEAFSNVSNEAKDFIRRLLIKNKEKRMTAHECLMHAWLRGDYSP-R
16	TR:E2BUG0_HARSA	57.6%	4926:5295	GVLAYVLLSGLSPFAGDNDIETLKNVKACDWDFDEEAFRDVSEEGKDFIRRLLVKNKEKRMTAHECLLHPWLT-GDHSKW
17	TR:Q7YT99_MYTGA	56.1%	3826:4197	GVLAYVLLSGLSPFAGEDDLETLANVQRCDWEFADDAFANISPEAKDFIRKLLIRQPQRRMTVHECLDHDWM-KGDLSGR
18	TR:B4NHW1_DROWI	57.1%	8205:8577	GVLAYVLLSGLSPFAGDNDVQTLKNVKACDWDFDLEAFRHISEEGKDFIRKLLLANKEKRMTAHECLLHPWLT-GDHSGL
19	TR:B5DRZ6_DROPS	56.6%	5199:5571	GVLTYVLLSGLSPFAGENDVQTLKNVKACDWDFDVESFRHISEEGKDFIRKLLLANKEKRMTAHECLLHPWLT-GDHSGL
20	TR:B4H896_DROPE	56.6%	7318:7690	GVLTYVLLSGLSPFAGENDVQTLKNVKACDWDFDVESFRHISEEGKDFIRKLLLANKEKRMTAHECLLHPWLT-GDHSGL
21	TR:B4JZU2_DROGR	56.0%	7845:8217	GVLAYVLLSGLSPFAGDNDVQTLKNVKACDWDFDVDAFRHISEEGKDFIRKLLLANKEKRMTAHECLLHPWLT-GDHSDL
22	TR:B3N0W9_DROAN	55.2%	7911:8283	GVLAYVLLSGLSPFAGDNDVQTLKNVKACEWDFDEQSFNNISDDGKDFIRKLLVANKEKRMTAHECLLHPWLT-GDHSNM
23	TR:D0Z7E3_DROVI	55.7%	7962:8329	GVLAYVLLSGLSPFAGDNDVQTLKNVKACDWDFDLEAFKHISDEGKDFIRKLLIASKEKRMTAHECLLHPWLT-GDHREL
25	TR:Q961U1_DROME	55.4%	728:1095	GVLSYVLLSGLSPFAGDNDVQTLKNVKACDWDFDVESFKYISEEAKDFIRKLLVRNKEKRMTAHECLLHPWLT-GDHSAM
30	TR:B4IIY8_DROSE	55.4%	1444:1811	GVLSYVLLSGLSPFAGDNDVQTLKNVKACDWDFDVESFKYISEEAKDFIRKLLVRNKEKRMTAHECLLHPWLT-GDHSAM
32	TR:B4PW26_DROYA	55.2%	7933:8300	GVLSYVLLSGLSPFAGDNDVQTLKNVKACDWDFDVESFKYISEEAKDFIKKLLVGNKEKRMTAHECLLHPWLT-GEHCAM
34	TR:Q17HV9_AEDAE	53.1%	6150:6524	GVLAYVLISGLSPFAGETDIDTLKNIKQGTWEFDEVAFKDVSEECKDFIRRLLIKNTEKRMTAHECLMHPWLS-DSYNSS
35	TR:E3WIY5_ANODA	52.3%	6975:7348	GVLAYVLVSGLSPFAGETDIDTLKNIKQGTWEFDEVAFRDVSEECKDFIRRLLIKNKEKRMTAHECLSHVWLS-DTYNSS
36	TR:Q7PXW9_ANOGA	52.0%	7186:7560	GVLAYVLVSGLSPFAGETDIDTLKNIKQGTWEFDEVAFRDVSEECKDFIRRLLIKNTEKRMTAHECLSHAWLS-DTYNSS
37	TR:B0W5W8_CULQU	51.7%	6148:6522	GVLAYVLISGLSPFAGETDIDTLKNIKQGTWEFDEVAFKDVSEECKDFIRRLLIKTKEKRMTAHECLMHAWLS-DSYNSS

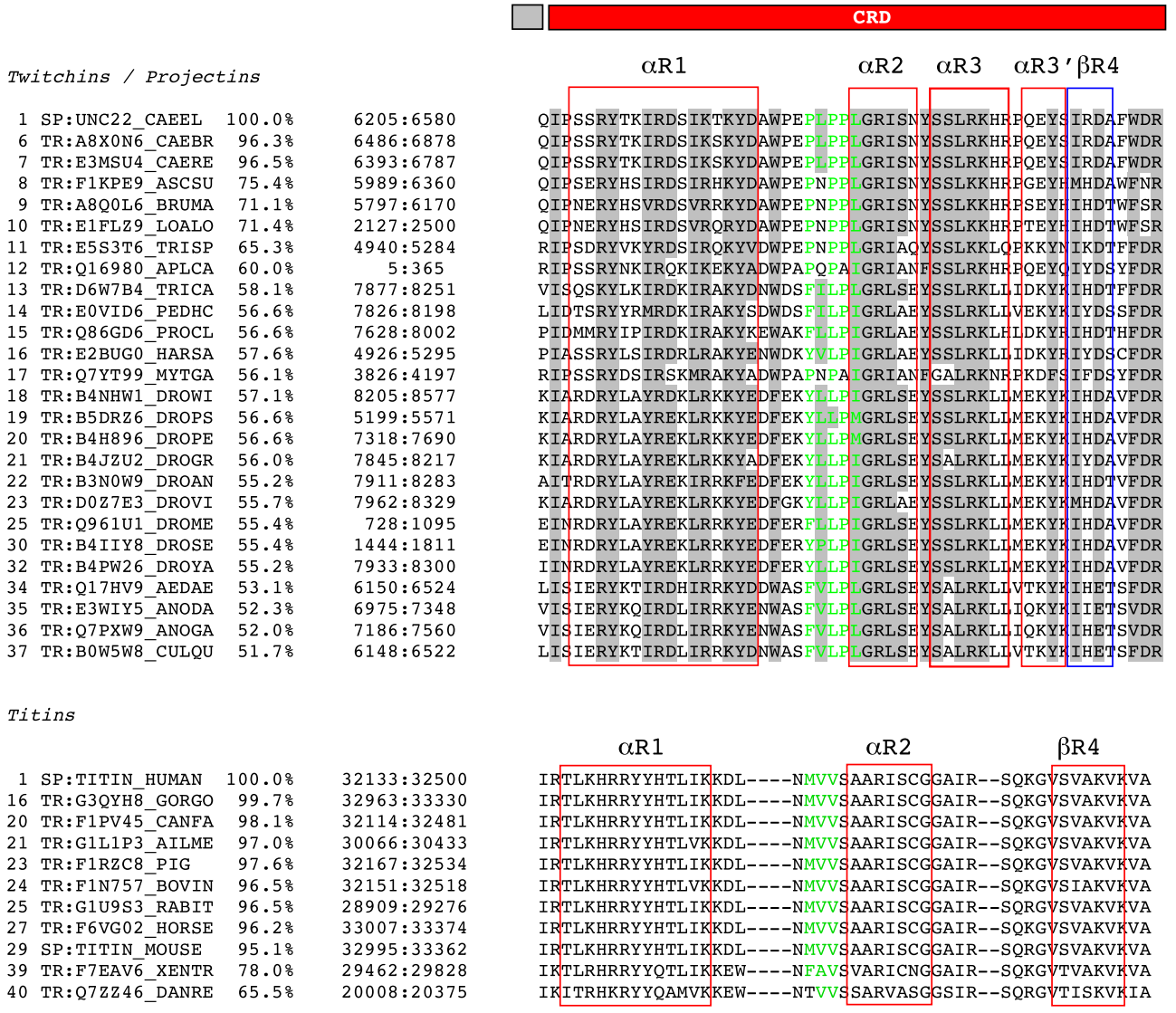

Fig. S3. Sequence alignment of the kinase regions of twitchins and projectins from nematodes, mollusks and insects. The alignment is annotated as to highlight the conservation of N- and C-terminal regulatory segments in twitchins and projectins. In the N-terminal linker region (NL), positively charged residues are colored blue, conservation in the β-strands of the β-hairpin loop is indicated in grey and defining features of the crown segment are in yellow. Tyrosine residues in the NL (or the structurally complementary region in sequences from mollusks) are marked in green as putative phosphorylation targets. The catalytic residue E201 in helix H3 of the kinase domain is shown in magenta. The motif of negatively charged residues in the βC4-βC5 loop is in red. In the CRD region, sequence conservation is shown in grey. Here, conserved groups are primarily located in secondary structure elements as well as in a final capping motif (with sequence FDR). Notably, the most C-terminal elements (i.e., the short αR3′ helix and strand βR4)—proposed in this study as the most mechanically labile parts of the CRD—exhibit little conservation. The loop joining αR1 and αR2 in twitchins/projectins is markedly hydrophobic (colored green). For comparison, NL and CRD sequences for several representatives of vertebrate titins are included. The sequence displayed starts right after the termination of the preceding Fn3 domain, A170, and a vertical line indicates the beginning of the kinase domain (domain boundaries as revealed by the crystal structures of human TK [PDB entry 1TKI] and the tandem A168-A170 [2NZI]). The absence of the positively charged motif and the β-hairpin loop in the NL region is prominent. The crown region lacks the aromatic motif and is highly charged, being rich in negative groups (red). In the CRD, helix αR3 is missing, loops are shorter and helix αR2 is rich in small Gly and Ala residues. (Given that the sequence conservation across vertebrate titins is noticeably high, this has not been highlighted).

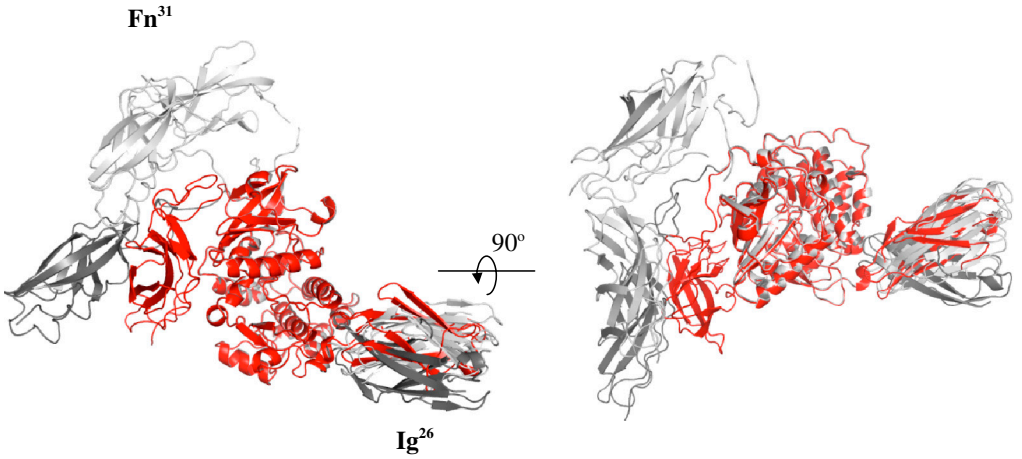

Fig. S4. Representative SAXS models calculated by rigid-body refinement. Orthogonal views are provided of a set of representative SAXS models (grey) calculated using rigid-body refinement in SASREF and superimposed on the crystal structure of twitchin comprising the domains Fn^{31}-Nlinker-kinase-CRD-Ig^{26} (TwcKR) (red). The SAXS models consisted of four rigid-body fragments—Fn^{31}, NL front region, kinase-CRD, and Ig^{26}—that had been allowed to migrate independently and unrestrained, with the proviso that the corresponding C and N termini of consecutive fragments should not drift further apart than 5 Å distance and that no steric overlap should occur between rigid-bodies. Models resulting from refinements with this high degree of freedom showed large variations in the positioning of domain Fn^{31}, while the arrangement of Ig^{26} was typically in good agreement with the crystallographic model (light grey). Even those models differing in the position of Ig^{26} (example shown in dark grey) did not deviate significantly. This result is probably due to the short linker sequence connecting the kinase-CRD module and Ig^{26}, which must limit the permitted relative arrangements of these domains. The variations affecting Ig^{26} were mostly in the form of rotations around its primary molecular axis. It should be borne in mind that the Ig fold has the overall shape of a prolate ellipsoid of rotation, with a long primary axis but an isometric cross-section. As a result, rotations around the primary axis yield little change in overall molecular shape and are poorly distinguishable by SAXS. Thus, the position of Ig^{26} in the resulting models is defined in the direction of the main axis, but poorly resolved in azimuthal orientations. Given (*i*) the good agreement of SASREF and crystallographic models in this region at the low resolution of the SAXS technique; and (*ii*) the good agreement of the Ig^{26} position between current and previous crystallographic models (3), we saw no impediment in fixing the position of Ig^{26} in subsequent cycles of SASREF studies. We then tested models in SASREF where the crystallographic kinase-CRD-Ig^{26} fraction had been kept as a single rigid-body. This restrain helped the scoring of Fn^{31} positions.

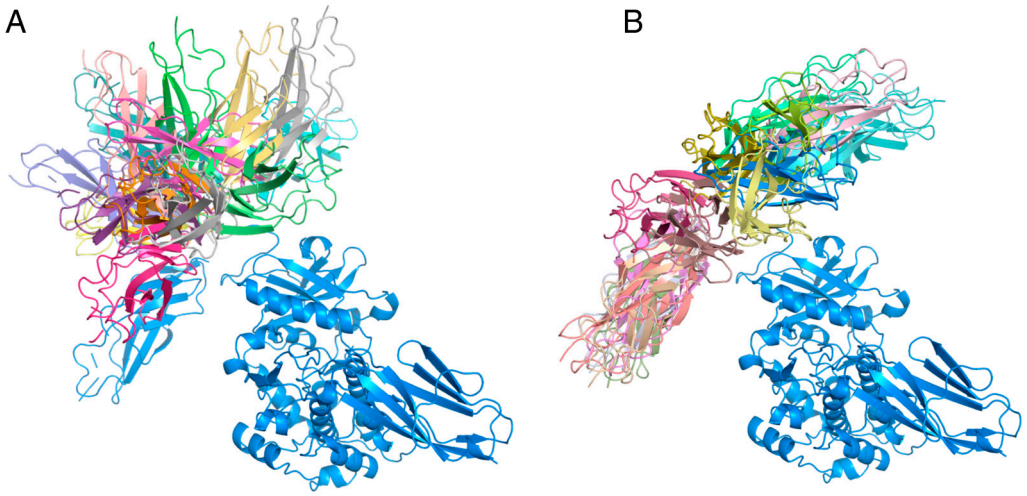

Fig. S5. EOM analysis of SAXS models. Structural diversity in SAXS models of TwcKR; (*A*) a set of representative models from a pool generated by randomly varying the junction between Fn^{31} and the N-linker; (*B*) a typical ensemble selected by EOM from the random pool. It should be noted that global molecular shapes where Fn^{31} is oriented at opposite rotational angles but with equivalent aperture angle are similar at low resolution and difficult to distinguish by SAXS.

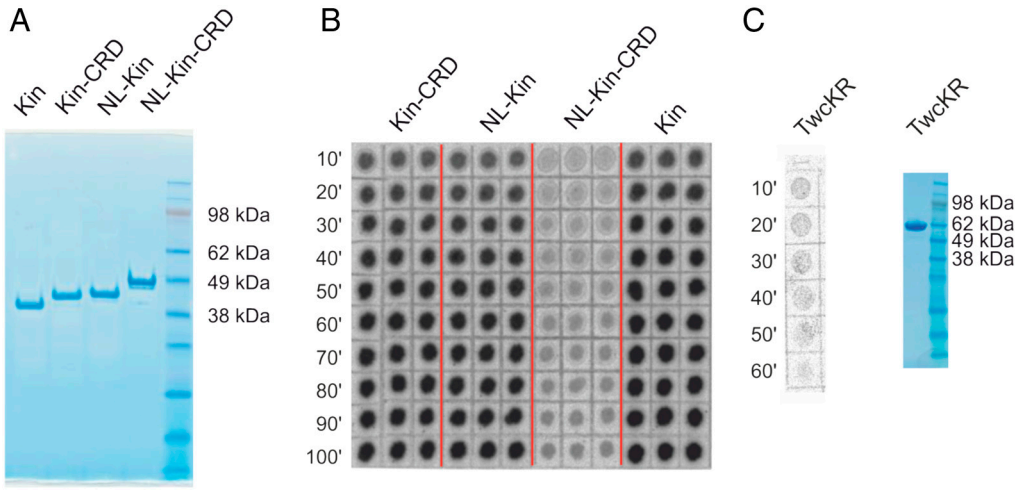

Fig. S6. Catalytic assays. (*A*) SDS-PAGE of purified kinase samples used in catalysis tests; (*B*) Spotted paper showing catalytic measurements (in triplicate) of TwcKR and subfragments on a MLCK-derived peptide substrate (see *Methods*). Sampling was at 10 min intervals; (*C*) Spot blots and SDS-PAGE of full-length TwcKR. Catalytic measurements of TwcKR were carried out in an independent experiment. The activity of both TwcKR and NL-kinase-CRD constructs was barely detectable and non-quantifiable.

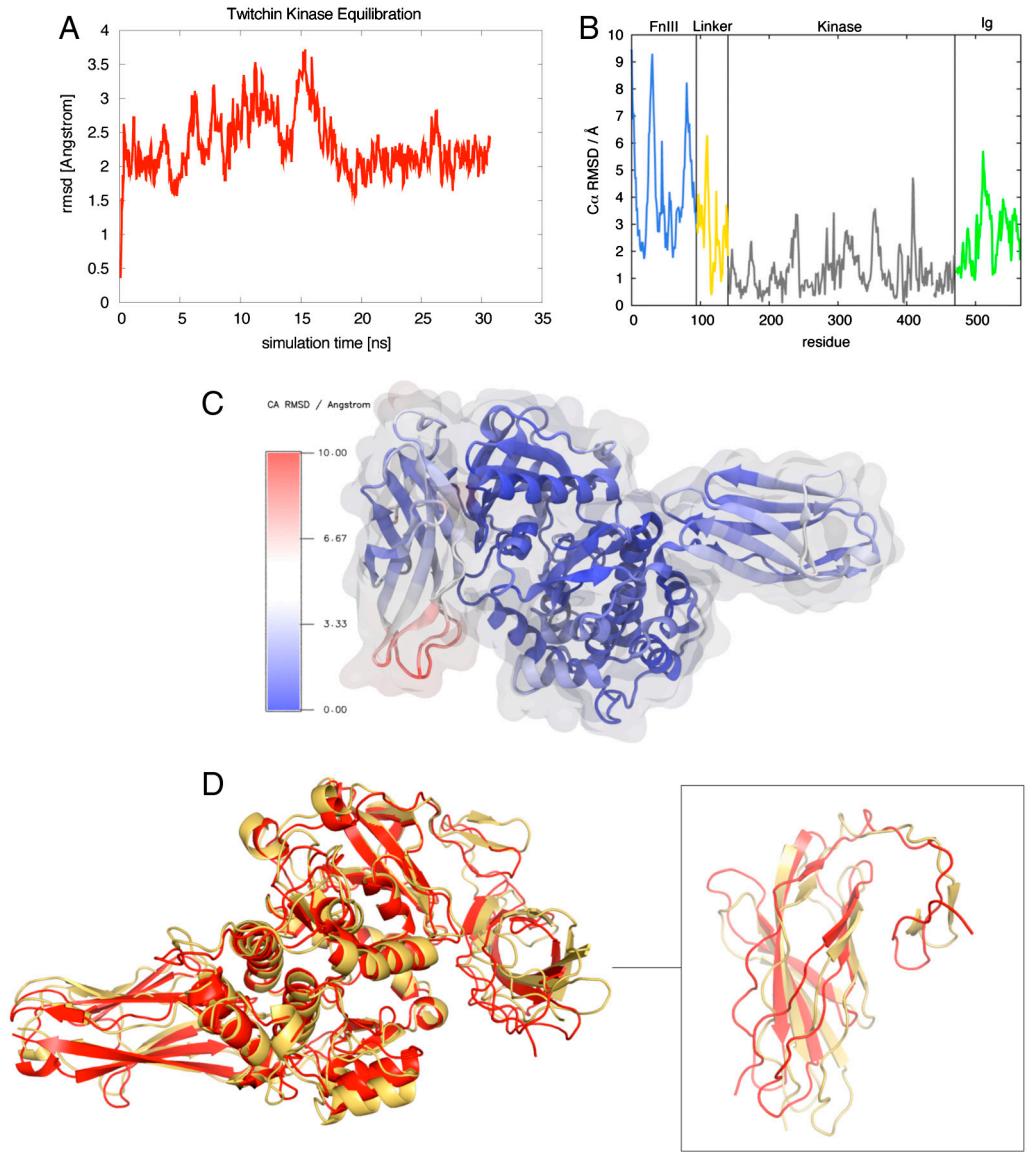

Fig. S7. Stability of the Fn^{31}/CRD interactions in Molecular Dynamics Simulations. (*A*) Variation of the overall rmsd between MD and crystallographic models over the equilibrium simulation (30 ns). The trace suggests that equilibrium is reached after 20 ns; (*B*) rmsd per residue resulting from the comparison of the equilibrated MD model and the crystal structure of TwcKR when superimposed on the kinase domain alone. The trace shows that domain Fn^{31} and the NL front undergo the largest variation, while shifts in domain Ig^{26} are only small; (*C*) rmsd per residue mapped onto the crystal structure of TwcKR. This plot shows that the biggest displacements in the structure occur at the apix of Fn^{31}; (*D*) Superimposition of the crystallographic (red) and MD (tawny) models. The comparison shows that the shift in domain Ig^{26} is limited to a small pivot motion around its single linker point to the kinase-CRD. Fn^{31} undergoes a more noticeable rocking motion. Positional variations in the domain are better appreciated in the *inset* (*Right*) that shows this region in isolation. As a result, the cluster of polar interactions (group *ii* in Fig. S2) is disrupted and no longer present in the MD equilibrated model, supporting the view that these are weak interactions and that the interaction of Fn^{31} with the kinase core is flexible. (It must be noted that the equilibrated MD state is unlikely to capture the full dynamics of this part of the molecule, which is probably far greater as indicated by SAXS).

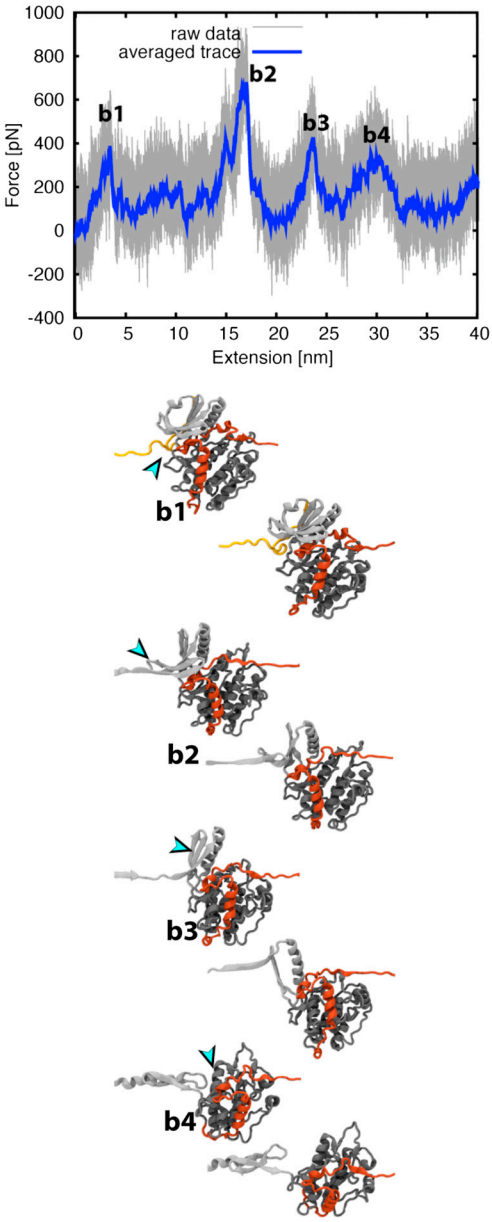

Fig. S8. Stretch response MD simulation on the isolated kinase core. Force extension curves (*Upper*) and stretch-induced conformational states corresponding to main mechanical events (*Lower*) in simulations of the NL-kinase-CRD fraction. The force peaks from primary unfolding events are labeled. Simulations were carried out until a molecular extension of approximarely 30% contour length was reached. As in full-length TwcKR, also here the force extension curve showed that the NL and the C-terminal elements of the CRD (strand βR4 and αR3′) unraveled first and at low force. As before, the further application of force caused the collapse of the N-terminal kinase lobe. The rest of the CRD, including helix αR2, remained firmly in place via interactions to the C-terminal kinase lobe and only unraveled after the N-terminal lobe had completely unfolded at 28 nm extension. The unfolding of the N-terminal kinase lobe occurred in three steps (FPb2-b4), where the two initial events (FPb2-b3) arise from the rupture of salt bridges and the third event (FPb4) results from the breaking of hydrogen bonds between strands βC3 and βC4. (Trajectory illustrated in Movie S3).

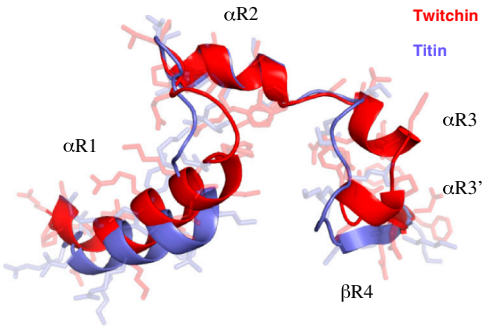

Fig. S9. Structural superimposition of the CRD regions of titin and twitchin kinases.

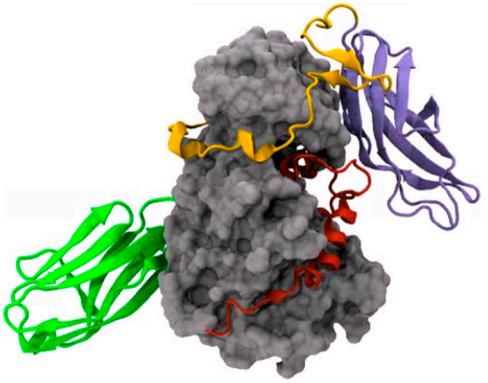

Movie S1. Crystal structure of TwcKR. (This video is an animation of Fig. 1*B* in the main text). Domains are color-coded as in Fig. 1 of the main text. Namely, domain Fn^{31} is shown in blue, the N-terminal linker is in yellow, the catalytic kinase domain is grey (surface representation), the C-terminal regulatory tail is red, and domain Ig^{26} green.

Movie S1 (AVI)

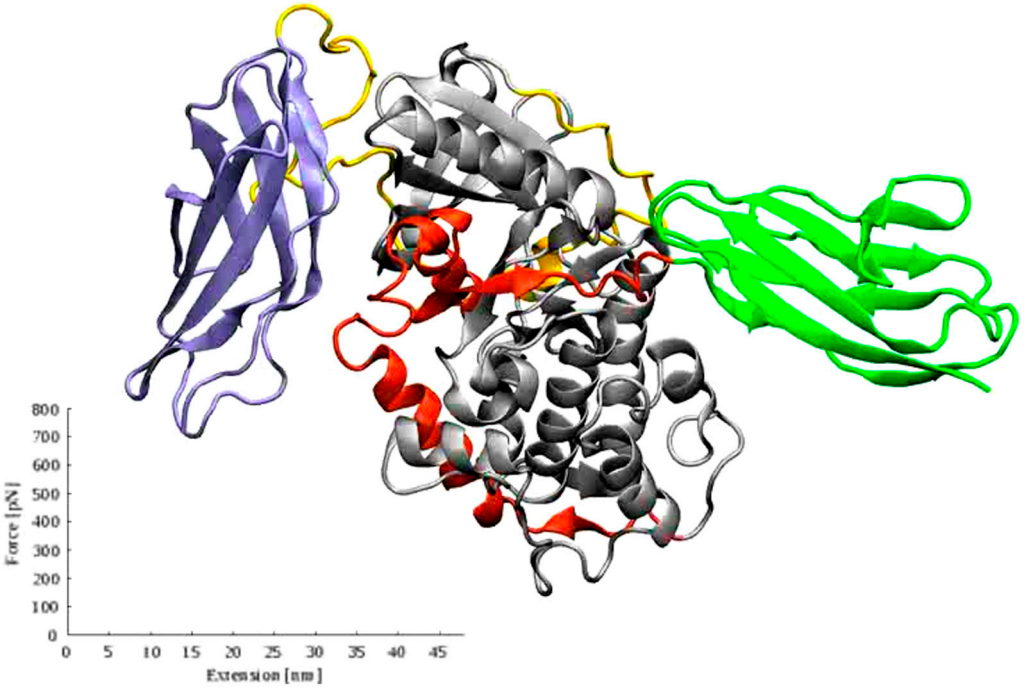

Movie S2. Steered Molecular Dynamics of TwcKR. (This video is an animation of Fig. 5 in the main text). Trajectory of structural transitions and corresponding force extension curve. Protein domains are color-coded as in Fig. 1 of the main text.

Movie S2 (AVI)

Movie S3. Steered Molecular Dynamics of the core region of TwcKR. (This video is an animation of Fig. S8 in *SI Text*). Trajectory of structural transitions and corresponding force extension curve.

Movie S3 (MOV)

Table S1. Specific interactions of the N-terminal regulatory region

Fn^{31}	Ct-RD	Distance (Å)
F12 [N]	E465 [OE2]	2.8
E92 [O]	R462 [NH1]	2.9
E92 [O]	R462 [NH2]	3.1
E92 [OE1]	E465 [N]	3.0
E92 [OE2]	Q464 [N]	2.9
P93 [O]	R462 [NH1]	3.2
Fn^{31}	Nt-Linker	Distance (Å)
D17 [ND2]	G116 [O]	3.4
I18 [O]	R104 [NH1]	3.8
D20 [O]	G101 [N]	2.8
D20 [OD1]	R104 [NE]	2.7
P100 [O]	D102 [N]	3.0
P100 [O]	E103 [N]	3.0
G101 [O]	R104 [N]	3.5
D20 [OD1]	R104 [NH2]	3.4
Kinase	N-linker	Distance (Å)
S234 [OG]	D130 [OD1]	2.5
K288 [N]	D130 [OD1]	3.0
R289 [N]	D130 [OD2]	3.7
T178 [OG1]	Y140 [OH]	3.5
N180 [ND2]	Y140 [OH]	2.9
Q203 [NE2]	V145 [O]	3.4
E221 [N]	K148 [O]	3.1
Y156 [N]	V152 [O]	2.8
R176 [NH2]	L153 [O]	2.7
R176 [N]	H155 [O]	2.7
D222 [OD2]	R108 [NH1]	3.3
E225 [OE2]	R120 [NE]	3.0
E225 [OE1]	R120 [NH2]	2.8
H159 [O]	K122 [N]	3.6
E160 [OE2]	Y129 [OH]	2.5
E175 [OE1]	Y140 [OH]	2.6
S206 [OG]	V145 [N]	2.9
A219 [O]	K148 [N]	3.0
D222 [OD2]	H151 [ND1]	3.7
Y156 [N]	H155 [O]	2.2
E225 [OE1]	R108 [NH1]	3.7
D222 [OD2]	R108 [NH1]	3.3
E225 [OE1]	R120 [NE]	3.7
E225 [OE2]	R120 [NE]	3.0
E225 [OE1]	R120 [NH2]	2.8
E225 [OE2]	R120 [NH2]	3.6
D218 [OD1]	K148 [NZ]	3.2
D222 [OD1]	H151 [ND1]	3.9
D222 [OD2]	H151 [ND1]	3.7

Calculated using PISA (http://www.ebi.ac.uk/msd-srv/prot_int/pistart.html).